Study of LiFi-Enabled UAV Swarm Networks

AHMET BURAK OZYURT[1,*], ILENIA TINNIRELLO[2], AND WASIU O. POPOOLA[1]

[1] Institute for Imaging, Data and Communications, School of Engineering, The University of Edinburgh, EH9 3JL Edinburgh, UK
[2] Department of Engineering, University of Palermo, 90128 Palermo, Italy
[*] a.b.ozyurt@ed.ac.uk

Compiled February 6, 2024

Unmanned aerial vehicle (UAV) swarm communication is a powerful component of aerial relays; however, conventional radio frequency (RF)-based UAV swarm networks struggle to ensure timely and reliable communication. To this end, a light spectrum-based wireless system, LiFi, is presented to supplement in this work thanks to its distinctive benefits. We present the analytical derivation of the average block error probability (ABEP) as Chebyshev approximation, lower and upper bounds. Then, the key performance metrics of reliability, throughput, and latency expressions are provided as a function of the ABEP. The results show that the severe requirements of ultra-reliable (99.99%) and low-latency (sub-millisecond) communication (URLLC) are satisfied at even low signal-to-noise ratio (SNR) values. Besides, in the numerical results, the impact of blocklength, packet size, the different distances among UAVs, SNR value, and light-emitting diode (LED) semi-angle are explored.

http://dx.doi.org/10.1364/ao.XX.XXXXXX

1. INTRODUCTION

In recent years, unmanned aerial vehicles (UAVs) or drones are getting more attention for important use cases, such as internet-of-things (IoTs), cooperative surveillance, disaster relief, and the defence industry [1]. In particular, employing more than one UAV or a UAV swarm as aerial relays can boost the capability of wireless communications rather than single-hop communications. However, in UAV-enabled relaying networks, timely and reliable communication among UAVs is needed to accomplish a series of missions accurately and effectively.

At Tokyo 2020 Olympics Opening Ceremony, more than 1800 drones configuring smoothly into a revolving planet Earth were one of the most talked about use cases of UAV swarm networks. In this scenario, the drones are specifically designed for entertainment purposes and are equipped with four light-emitting diodes (LEDs) that relay light that is true to colour and unmatched in brightness and vibrancy [2]. When we consider such a massive scenario, it is difficult to achieve reliable and timely communications among the UAVs and effectively suppress the loss of wireless channels for information delivery. To improve the performance, utilizing certain drones as relay nodes and exploring the potential of the infrared/visible light spectrum as a communication channel can prove to be advantageous at this stage. In this article, LiFi-enabled UAV swarm relaying is seen as the entry point to improve the performance of networks.

The current level of latency and reliability in UAV relay systems are not adequate for upcoming UAV swarm systems because they are mainly designed for manual remote control or preprogramming [3]. However, autonomous UAV swarms are emerging as a novel technology and need latency-intolerant control because they have to make real-time or near-real-time decisions [4]. Even slight delays in avoiding collisions and obstacles could cause dangerous consequences. According to the 3rd Generation Partnership Project (3GPP) Technical Report 22.862, the upper bound of latency for air-to-air radio links is determined as 5 ms, so the flight controller can have good responsiveness for gesture control. In addition, most of the low latency required services are inseparable parts of ultra-high reliability [5]. As examples of scenarios demanding low latency and ultra-high reliability services for UAV swarm networks, we can consider applications in various domains, including natural disasters, industrial automation, military operations, and agriculture [6]. In disaster situations, terrestrial communication networks may suffer disruptions, resulting in isolated sub-networks. To address this, temporary communication infrastructure using UAV swarm networks becomes essential to bridge the connectivity gaps. In such critical circumstances, maintaining a reliable communication network through fast network repair is crucial for the efficient dissemination of emergency information between victims and first responders [7]. For time-sensitive industrial IoT applications, such as remote control, intelligent robots, and personal health monitoring, UAV-based communication offers advantages [8]. UAVs can establish direct links with high probability and dynamically adjust their positions in response to environmental changes, thereby improving channel quality and ensuring seamless communication. In military operations, a central controller may need to transmit command information to a distant UAV carrying out reconnaissance missions in a military area. However, the presence of concealment structures with thick cement or metal walls poses challenges to direct communication. In such scenarios, UAVs equipped with ultra-reliable and low-latency communication (URLLC) capabilities can fly above the shelter, acting as intermediaries to facilitate the transmission between the controller and the distant UAV. In the context of agriculture, the automation of the farm ecosystem is a critical objective. URLLC-enabled UAVs play a pivotal role in achieving this goal by enabling real-time farm management. The high degree of automation enhances food safety, improves the efficiency of the food supply chain, and optimizes the utilization of natural resources [9]. By presenting these application scenarios, our research underscores the significance of URLLC for UAV swarm networks across diverse domains.

The conventional UAV swarms need to tackle some problems, e.g., radio frequency (RF) spectrum crunch, energy consumption, mutual interference, and pricey components. Moreover, the ubiquitous use of UAVs will disrupt cellular networks seriously because the suggested sub-6 GHz spectrum for UAVs is massively utilized by cellular networks. The operation of UAV swarms in the sub-6 GHz spectrum can decrease their system capacity more than the planned level; thus, it can dramatically affect the quality of service for ground users [1]. Also, another challenge for a UAV swarm is energy efficiency, and the battery is one of the most precious resources.

A UAV swarm needs reliable data transmission among its members via a local wireless network such as for cooperative communications. In this regard, WiFi, LoRa, and ZigBee are suggested by the standards community as non-3GPP technologies to support the emerging UAV swarm use cases [4]. When this suggestion is taken into account, the introduction of LiFi, a light-spectrum-based wireless system, as a non-3GPP technology can be featured due to its advantages in communication among UAVs. The LiFi channel is more directional, with less and in many setups negligible multi-path propagation, and without small-scale fading. Interference in the RF case can be avoided in hybrid RF/LiFi networks due to their different operating frequency bands [10]. Thus, the LiFi-enabled technique ensures the relaying is in a deterministic way which may enable better reliability and low-latency. The front-end components of LiFi are relatively simple transmitters and receivers. Due to operation in the baseband, no need for frequency mixers or sophisticated algorithms for the compensation of RF impairments, such as IQ imbalance and phase noise [11]. The implementation cost of the LiFi is expected to be lower than conventional technologies because optical components are less expensive than the existing RF front ends. Light transmitters are also energy-efficient sources and using them can achieve higher energy efficiency for UAV swarms [12]. The availability of this unlicensed spectrum for UAV swarms helps to decrease the overall cost. As an important point, the proposal of LiFi technology in this work is not to completely replace the RF technology in the UAV swarm networks. Mitigating communication bottlenecks caused by the nature of the RF spectrum is the main challenge addressed here.

A. Related Works

Considering the scope of this study, we can mainly categorize the related works about UAV communications in terms of their spectrum regions into two groups which are radio frequency (RF) and optical band.

As discussed in the previous section, URLLC is an important technology for UAV communication but also there are still challenges to be addressed. Most of the studies in the RF spectrum focus on multi-objective optimization which involves minimizing or maximizing multiple objective functions subject to a set of constraints. In particular, joint optimization of the UAV's location, antenna beamwidth, transmit power, blocklength, device association, energy efficiency, resource allocation, decoding error probability or transmission rate is considered for various scenarios such as agriculture, edge computing, internet-of-things (IoT), free space path, 3-dimensional channel [9, 13–24]. These joint optimization problems are formulated subject to strict reliability and latency requirements, the total bandwidth for URLLC or finite blocklength regime, and solved by iteration algorithm, ions motion algorithm, mixed integer nonlinear program, bisection search, block coordinate descent, Lagrange dual decomposition techniques, deep neural network based algorithm, perturbation based iterative algorithm. Another approach in previous works presents analytical expressions for providing deeper insights into the system design[7, 8, 25]. In [7] and [25], the average achievable data rate (AADR) or the average packet error probability (APEP) and effective throughput (ET) of the control information delivery from the ground control station (GCS) to the UAV under free space or 3-D channel are derived. Also, the idea is to deploy multiple UAVs for acting as a relay between the ground transmitter and the flying UAV base station is proposed for increasing reliability [26]. The current state-of-art on URLLC-enabled UAV networks in the RF domain is detailed in [6].

Secondly, the previous studies benefited from optical bands to tackle problems of conventional technologies such as RF spectrum scarcity, interference, and network connectivity. However, most studies in optical bands introduced the same type of multi-objective optimization problems as the previous RF studies. To maximize the received data and the user cluster size, the optimization problem of joint user association and deployment location of UAVs for two-tiered visible light communication networks is analyzed in [27]. In [28–30], the cell associations and the locations of UAVs are optimized according to communication constraints for maximizing energy efficiency. In another study, the blocklength allocation and UAV deployment with alternating direction method of multipliers are jointly optimized for minimizing total error probability [31]. Energy and user mobility aware three-dimensional deployment of visible light communication (VLC)-enabled UAV-base station is also introduced; thus, achieving maximum coverage of users while ensuring fairness [32]. In [1], ultraviolet (UV) communication is exploited to address the problems of RF spectrum scarcity, interference, and network connectivity for UAV swarm communication. Further, the system performance is investigated in terms of data rate and communication range.

B. Contributions and Outline

In this paper, we investigate infrared/visible bands-based LiFi technology for enabling strict reliability and latency requirements in UAV-enabled relaying networks. The contributions are as follows:

1. For the first time in the literature, we introduce the use of LiFi signals for URLLC-constrained relay systems among UAVs due to the deterministic and accurate nature of the infrared/visible light channel, energy efficiency, low implementation cost and spectrum availability.

2. We model the statistical characteristics of the signal-to-noise ratio (SNR) for the LiFi-based swarms by assuming that the UAVs fly freely in an area.

3. We then study the average block error probability (ABEP) under short packet transmission in LiFi systems for the relay system among UAVs. The Chebyshev approximation, lower and upper bounds are derived to obtain the ABEP for providing insight into the packet size and system design.

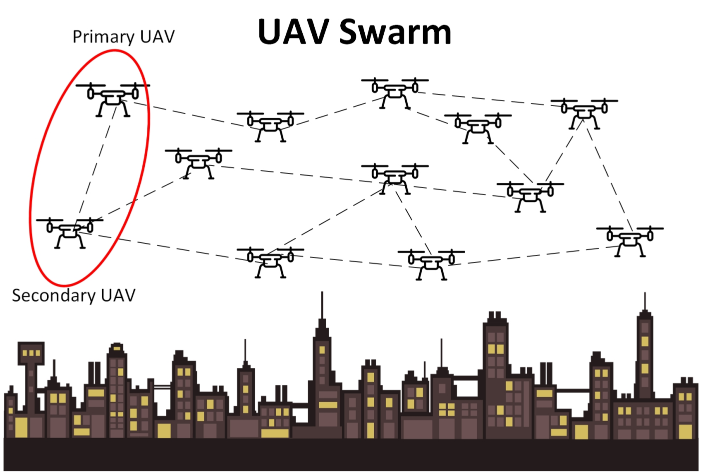

Fig. 1. Illustration of the LiFi-based UAV swarm communication system - example scenario.

4. By leveraging the obtained ABEP expressions, we show the different boundaries of reliability, latency, and throughput for URLLC-constrained relay systems in UAV swarms.

5. Extensive Monte-Carlo based simulations presented to validate the analytical model.

The rest of this paper is organized as follows. The network model, LiFi channel model, and short packet transmission in LiFi systems are introduced as parts of the system model in the next section. In Section 3, the Chebyshev approximation, lower bound, and upper bound of the ABEP and performance metrics are presented. Simulation results and analysis are shown in Section 4. Finally, we give the concluding remarks in Section 5.

2. SYSTEM MODEL

This section provides the LiFi-based UAV swarm system model which is used in the study. Firstly, the UAV swarm deployment and orientation model are provided in line with the previous studies [7, 25, 33, 34]. Secondly, the details of the LiFi channel model used among UAVs are given. Then, short packet transmission in the LiFi system is presented.

A. Network Model

This study focuses on relaying systems under ultra-reliable and low-latency constraints among UAVs in a swarm network rather than data transmission between ground users and UAVs as in previous studies. Thus, the topology of LiFi-based UAV swarm networks is considered in this section. Actually, the absence of accurate multi-swarm UAV deployment models, especially those operating in optical bands, is a key difficulty in investigating the performance of this type of network. Thus, we consider a UAV swarm network such as in Fig. 1. In the presented configuration, each UAV is equipped with an array of LEDs and photodiodes, positioned in a quadrangular arrangement on a panel, as illustrated in Fig. 2 and applied in other works [7, 25, 33]. LEDs and photodiodes have been strategically placed, with one set located at the bottom of the UAV panel and another at the top. The remaining two optical devices are arranged in a diagonal pattern along the edges of the wings. The transmission and reception of the bit stream occur through the LiFi front-ends, namely the LED and the photodiode. On the transmitter side, a circuit driver is employed to transform the received voltage signal into a current signal, subsequently driving the LED for light emission. Conversely, on the receiver side, the modulated light signal is captured and transduced back into an electrical signal through the photodiode. This arrangement facilitates the bidirectional exchange of information between UAVs through LiFi channels. The primary UAV is located at the centre of the sphere and the secondary UAV is assumed to be within the outer sphere to ensure that the UAVs are within the control range. Also, since there will be minimum distance among UAVs, the radius of the inner and outer spheres are shown as D_{min} and D_{max}. As the UAV may fly anywhere within the region, the directions of the UAV movements are uniformly distributed.

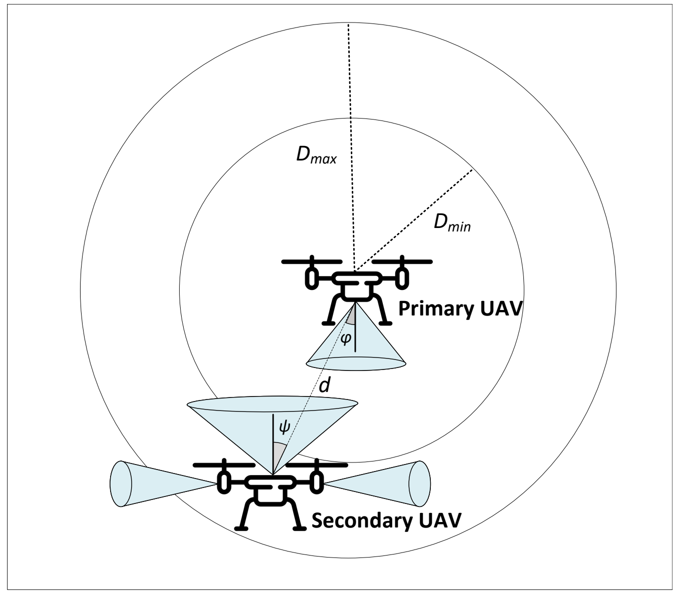

Fig. 2. The ultra-reliable and low-latency transmission of control signal from the primary UAV to the secondary UAV.

Then, the cumulative distribution function (CDF) of the distance, d between the primary UAV and the secondary UAV is [7]:

$$F_d(x) = \frac{x^3 - D_{min}^3}{D_{max}^3 - D_{min}^3}, \; D_{min} \leq x \leq D_{max} \tag{1}$$

and the probability distribution function (PDF) is

$$f_d(x) = \frac{dF_d(x)}{dx} = \frac{3x^2}{D_{max}^3 - D_{min}^3}, \; D_{min} \leq x \leq D_{max}. \tag{2}$$

The use of the uniform UAV distribution model aligns with the existing literature, particularly in the context of several UAV swarm network studies to which our model is adapted [7, 25, 33]. This approach permits the modeling of UAV speed as a random distribution rather than being constrained to a single fixed value during the assessment of system performance. Incorporating this modeling strategy simplifies the analysis of UAV mobility's influence on LiFi networks, thereby yielding realistic insights for the design of robust and dependable LiFi networks.

Moreover, the UAVs were deployed at a relatively low altitude during the experiment to ensure stable and controllable flight. To maintain the drones in relatively stationary positions between the drone planes, we employed position-hold and altitude-hold modes using advanced flight control systems. The use of such flight modes highlights the significance of latency-intolerant systems, which are a key focus of this research. These systems necessitate real-time or near-real-time decision-making capabilities, as emphasized in our proposed approach.

B. LiFi Channel Model

The UAVs in a swarm are more likely to establish short-distance line-of-sight (LoS) communication links. Moreover, the UAV swarm is designed for outdoor missions, so the effect of multiple reflections is neglected. This means that only LoS is taken into account for the LiFi channel model in this study. In addition, LEDs (Lambertian source) are assumed as the transmitters.

The UAV orientation significantly affects the signal quality of LiFi-based swarm networks contrary to conventional RF-based networks. However, modelling UAV orientation is extremely complex and dynamic due to various environmental factors such as atmospheric pressure, winds, moisture and venturi effect. This work will not focus on improving such an orientation model. Instead, the experimental model in [34] for LiFi-based devices was adapted to this study due to a lack of a proper UAV orientation model. According to this model, the LoS LiFi channel gain with respect to orientation among UAVs in a swarm can be expressed as [34]:

$$H = \frac{(m+1)A_r}{2\pi d^2}\cos^{m+1}(\psi)T_s g(\psi), \quad (3)$$

where d shows the distance among the UAVs, A_r is the receiver effective area, ψ is the angle of incidence with respect to the axis normal to the receiver surface, ψ_{con} is the field-of-view (FOV), $g(\psi)$ is the concentrator gain, T_s is the filter transmission, respectively, and m_i is the Lambertian index described as [10]:

$$m = -\frac{\ln(2)}{\ln[\cos(\varphi_{1/2})]}, \quad (4)$$

where $\varphi_{1/2}$ is the semi-angle at half illuminance of the transmitter. Further, the gain of the optical concentrator at the receiver is expressed by [10]:

$$g(\psi) = \begin{cases} \eta^2/\sin^2(\psi_{con}), & \text{if } 0 < \psi \leq \psi_{con} \\ 0, & \text{if } \psi_{con} \leq \psi, \end{cases} \quad (5)$$

where η is the refractive index.

For simplicity, in [34], it is assumed that $g(\psi) = T_s = 1$ and the angle of irradiance with respect to the axis normal to the transmitter surface, φ, is not affected by the random orientation due to the relative movement scenario. Thanks to this assumption, the complex multiple UAV movements scenario is simplified to a single UAV movement, which makes easier the analysis while still keeping the realistic features. The transmitter and receiver are aligned such as in Fig. 2. For the LiFi signaling among the UAVs, we consider an orthogonal frequency-division multiple access (OFDMA) scheme where each link is a unique slice of the optical spectrum. In this case, the LiFi links in the swarm can coexist without suffering interference from each other. Moreover, from the perspective of the spectrum, the available bandwidth of infrared/visible light is much larger than RF, which can eliminate the interference caused by the repeated use of RF spectrum resources in the UAV swarm. Therefore, the intra-group interference among UAVs is not considered in this paper.

To this end, the received SNR among the UAV in the swarm is given by $\gamma_r = (P_t H R_p e^{-\tau_{od}})^2/\sigma^2$, where P_t is transmitted optical power, R_p is photodiode responsivity, $e^{-\tau_{od}}$ is atmospheric absorption losses and σ^2 is zero-mean additive white Gaussian noise (AWGN) [10].

In a LiFi system, the total noise can be given as:

$$\sigma^2 = \sigma_t^2 + \sigma_s^2 \quad (6)$$

where σ_t^2 symbolizes the thermal noise variance which is constant and independent of the optical power. While, σ_s^2 denotes the shot noise variance which depends on the received optical power. The shot and thermal noise variances are defined as, $\sigma_t^2 = \frac{8\pi\kappa T_k}{G_{ol}} C_{pd} A_r I_2 B^2 + \frac{16\pi^2\kappa T_k \Gamma}{g_m} C_{pd}^2 A_r^2 I_3 B^3$, and, $\sigma_s^2 = 2qB(P_0 + I_B I_2)$, respectively, where, the bandwidth of the electrical filter that follows the photodiode is represented by B Hz, κ is the Boltzmann's constant, I_B is the photocurrent due to background radiation, T_k is absolute temperature, G_{ol} is the open-loop voltage gain, C_{pd} is the fixed capacitance of photodiode per unit area, Γ is the FET channel noise factor, g_m is the FET transconductance and noise-bandwidth factors, I_2 = 0.562, and I_3 = 0.0868 [10]. Furthermore, it is worth noting that the amount of sunlight received by UAV surfaces fluctuates between day and night scenarios, and this variability is influenced by the predominant light frequency. However, the accurate prediction of the spatial and temporal distribution of illumination necessitates the consideration of both sequential and spatial information, which falls beyond the scope of this work. It is generally assumed that sunlight could halt the operation of the communication system entirely due to interference. However, the effect of solar irradiance is more apparent as a strong shot noise source rather than an interference source as the sunlight intensity does not vary greatly over short periods of time [35]. Additionally, this shot noise effect is suitably approximated by a Gaussian distribution [36]. As a result, the effect of sunlight has been represented through the modeling of white Gaussian noise, as depicted in equation (6). For forthcoming derivations, we also denote the received SNR expression as $\gamma_r = (Wd^{-2})^2 = (\frac{P_t R_p e^{-\tau_{od}}}{\sigma})^2 H^2$, where $W = P_t R_p e^{-\tau_{od}} \frac{(m+1)A_r}{2\pi\sigma}\cos^{m+1}(\psi)$.

It is assumed that the UAVs are equipped with transmitters and receivers like in Fig. 2, as in previous works [1, 37–39]. A link within the best distance among neighbour UAVs realises the communication. This study evaluates the average link performance in a swarm and provides insights for future studies to consider enhancing the overall performance of the swarm. The LiFi-based UAV swarm communications are proposed as a stand-alone solution in certain environments or complementary to any existing RF solution in a general environment.

The blocking of the propagation path among UAVs is an important issue that needs to be resolved. Advanced techniques exist to mitigate the blocking issue in LiFi signal transmission. One promising approach involves leveraging reflective surfaces to redirect optical signals around obstacles. This technique is similar to the use of mirrors for redirecting light in a room and to the use of reflective intelligence surfaces (RIS) in the optical bands. Another approach is to use multiple optical transceivers to create a mesh network, where signals can be routed through multiple paths to avoid obstacles. Additionally, an airy beam can be used, which is a propagation-invariant wave whose main intensity lobe propagates along a curved parabolic trajectory while being resilient to perturbations [10].

C. Short Packet Transmission in LiFi Systems

Designing an ultra-reliable communications system for UAV swarms requires short packet communication (SPC) as a method in 5G and beyond. The SPC is expressed as the packet length or the number of codewords should be small to ensure the stringent latency for the URLLC-constrained relay systems. At this point, the Shannon capacity theorem cannot be adopted in this system model because of finite channel blocklength [40].

In this work, one of the most widely used optical modulation schemes, direct current biased optical orthogonal frequency division multiplexing (DCO-OFDM), is preferred. In DCO-OFDM, a direct current bias is added to generate a unipolar signal. In addition, to realise a real-valued OFDM waveform, Hermitian symmetry is imposed on the subcarriers of the OFDM frames. The packet size is L bits, which should be transmitted within T_{max} seconds. Then, the number of bits per channel used is given by $M = BT_{max}$. The coding rate is given by $R = L/M$ and an approximation of the block error probability (BEP) for LiFi system under finite blocklength transmission is given by [41]:

$$\varepsilon = Q(f(\gamma_r)), \tag{7}$$

where $f(\gamma_r) = \sqrt{\frac{M}{0.5V(\gamma_r)}}(0.5\ln(1+\gamma_r) - R_s)$, $R_s = \frac{L\ln 2}{M}$ (nats per channel use, or npcu), $V(\gamma_r)$ is the channel dispersion (variance of the information density achieved by a capacity-achieving distribution [42]) that is given by $V(\gamma_r) = 1 - (1+\gamma_r)^{-2}$, and $Q(x)$ is the Gaussian Q-function.

In the following section, we will obtain the different BEP values by considering the suggested scenario. The complex expression of ε in (7) makes the analysis of the BEP a challenging task.

3. BLOCK ERROR PROBABILITY AND PERFORMANCE METRICS FOR LIFI-BASED UAV SWARM NETWORKS

In this section, we will aim to derive the average BEP (ABEP) for intra-swarm communications under strict reliability and latency requirements. However, we need to first obtain the PDF of the SNR. Specifically, the ABEP for this system model is defined as

$$\bar{\varepsilon} = \mathbb{E}\{\varepsilon\} = \int_{D_{min}}^{D_{max}} \varepsilon f_d(x)dx, \tag{8}$$

where $\mathbb{E}$ is expectation, $f_d(x)$ is the PDF of d which is obtained in (2) and ε is provided in (7). As a next step, we need to derive the PDF of γ_r because ε includes its value as seen from (7). Thus, the CDF of γ_r can be given

$$F_{\gamma_r}(x) = \mathbb{P}\{\gamma_r \le x\} = 1 - \mathbb{P}\{d \le \sqrt[4]{W^2/x}\}. \tag{9}$$

By combining (1) and (9), the CDF of γ_r can be obtained as follows

$$F_{\gamma_r}(x) = 1 - \frac{(W/\sqrt{x})^{3/2} - D_{min}^3}{D_{max}^3 - D_{min}^3}, \gamma_{r_{min}} \le x \le \gamma_{r_{max}}. \tag{10}$$

Thus, we can take the first-order derivative of (10) to obtain the PDF of γ_r

$$f_{\gamma_r}(x) = \frac{3\,W^{3/2}x^{-4}}{D_{max}^3 - D_{min}^3},\ \gamma_{r_{min}} \le x \le \gamma_{r_{max}} \tag{11}$$

where $\gamma_{r_{min}} = (W/D_{max}^2)^2$ and $\gamma_{r_{max}} = (W/D_{min}^2)^2$. Finally, we can express the ABEP by using (7) and (11)

$$\begin{aligned}\bar{\varepsilon} &= \int_{\gamma_{r_{min}}}^{\gamma_{r_{max}}} Q\left(\sqrt{\frac{M}{0.5V(x)}}\left(\frac{\ln(1+x)}{2} - R_s\right)\right) f_{\gamma_r}(x)dx,\\ &= \frac{3W^{3/2}}{2(D_{max}^3 - D_{min}^3)}\\ &\quad\times \int_{\gamma_{r_{min}}}^{\gamma_{r_{max}}} \operatorname{erfc}\left(\sqrt{\frac{M}{V(x)}}\left(\frac{\ln(1+x)}{2} - R_s\right)\right)x^{-4}dx,\end{aligned} \tag{12}$$

where the last equality follows by using the relationship of erfc(x) $= 2Q(\sqrt{2}x)$.

To the best of the authors' knowledge, deriving a closed-form expression for (12) is a challenging task. Consequently, this study introduces three distinct approximations. Within UAV swarm networks, characterized by dynamic environmental conditions and variable system parameters, the application of Chebyshev approximation emerges as a valuable tool for performance assessment without relying on specific distribution assumptions. In statistical analysis, Chebyshev approximation is frequently employed to establish bounds on the probability that a random variable deviates from its mean beyond a specified threshold. The second approach involves an upper bound, portraying the system's worst-case performance scenario. It provides an upper limit on the anticipated error probability, a critical requirement for estimating the system's behaviour under adverse or extreme conditions while the third approach is a lower bound.

A. Chebyshev Approximation

To address the issue in (12), we apply Gaussian-Chebyshev quadrature to adress this issue by using Equation (25.4.30) in [43]. We define

$$q(x) = \operatorname{erfc}\left(\sqrt{\frac{M}{V(x)}}\left(\frac{\ln(1+x)}{2} - R_s\right)\right)x^{-4}. \tag{13}$$

Thus, (12) can be expressed in terms of (13) as

$$\begin{aligned}\bar{\varepsilon} &= \frac{3W^{3/2}}{2(D_{max}^3 - D_{min}^3)} \int_{\gamma_{r_{min}}}^{\gamma_{r_{max}}} q(x)dx,\\ &\approx \frac{3W^{3/2}(\gamma_{r_{max}} - \gamma_{r_{min}})}{4(D_{max}^3 - D_{min}^3)}\\ &\quad\times \sum_{i=1}^{N} a_i q\left(\frac{\gamma_{r_{max}} - \gamma_{r_{min}}}{2}t_i + \frac{\gamma_{r_{max}} + \gamma_{r_{min}}}{2}\right)\\ &\triangleq \bar{\varepsilon}_C.\end{aligned} \tag{14}$$

where t_i is the i-th zero of Legendre polynomials, N is the number of terms, a_i is the Gaussian weight given by Table (25.4) in [43]. The increase in N can increase the accuracy of (14), but at the cost of more computations.

B. Lower Bound

In the following, we aim to derive the lower bound of the ABEP for LiFi-based UAV swarm networks in closed form. To this end, we employ Jensen's inequality which is defined as $\mathcal{J}(f, X \sim \mathcal{P}) = \mathbb{E}[f(X)] - f(\mathbb{E}[X])$, where X is a random variable with distribution $\mathcal{P}$, and the function f might be convex or nonconvex [44]. According the inequality, we can obtain the lower bound of the ABEP as follows:

$$\bar{\varepsilon} = \mathbb{E}\{\varepsilon(\gamma_r)\} \ge \varepsilon(\mathbb{E}\{\gamma_r\}) \triangleq \bar{\varepsilon}_L. \tag{15}$$

For obtaining the value of $\bar{\varepsilon}_L$, we need to first calculate $\mathbb{E}\{\gamma_r\}$. From (11), we can calculate $\mathbb{E}\{\gamma_r\}$ as

$$\begin{aligned}\mathbb{E}\{\gamma_r\} &= \int_{\gamma_{r_{min}}}^{\gamma_{r_{max}}} f_{\gamma_r}(x)x dx \\ &= \int_{\gamma_{r_{min}}}^{\gamma_{r_{max}}} \frac{3\,W^{3/2}x^{-4}x}{(D_{max}^3 - D_{min}^3)}dx \\ &= \frac{3\,W^{3/2}}{2(D_{max}^3 - D_{min}^3)\gamma_{r_{max}}{}^2} - \frac{3\,W^{3/2}}{2(D_{max}^3 - D_{min}^3)\gamma_{r_{min}}{}^2}. \end{aligned} \quad \textbf{(16)}$$

Then, by using (7) and (15), $\bar{\varepsilon}_L$ can be easily expressed as

$$\bar{\varepsilon}_L = \varepsilon\left(\frac{3W^{-5/2}(D_{max}^8 - D_{min}^8)}{2(D_{max}^3 - D_{min}^3)}\right). \quad (17)$$

Even, when we consider that $W \gg 1$, $\bar{\varepsilon}_L$ in (17) can be further simplified as

$$\bar{\varepsilon}_L = Q(\sqrt{2M}(\ln(W^{-5/2}Y)/2 - R_s)), \quad (18)$$

where $Y = \frac{3(D_{max}^8 - D_{min}^8)}{2(D_{max}^3 - D_{min}^3)}$.

C. Upper Bound

In high SNR region, we can denote the upper bound of the ABEP, which is especially when $W \gg 1$ and $x \gg 1$. Thus, we have the following approximations $\log(1+x) \approx \log(x)$ and $\sqrt{V(x)} = \sqrt{1 - \frac{1}{(1+x)^2}} \approx 1$. (12) can be written as

$$\begin{aligned}\bar{\varepsilon}_U =& \frac{3W^{3/2}}{2(D_{max}^3 - D_{min}^3)} \\ &\times \int_{\gamma_{r_{min}}}^{\gamma_{r_{max}}} \text{erfc}\left(\ln 2\sqrt{M}\left(\frac{\log_2(x)}{2} - \frac{L}{M}\right)\right)x^{-4}dx \\ =& \frac{3W^{3/2}}{2(D_{max}^3 - D_{min}^3)}(z(\gamma_{r_{max}}) - z(\gamma_{r_{min}})), \end{aligned} \quad \textbf{(19)}$$

where the last equality is obtained by variable substitution. The function z can be approximated using Wolfram Mathematica Tool [45] as

$$\begin{aligned} z(x) =& -\frac{2}{3}e^{-(3(L\ln 16 - 3))/4M}\text{erf}\left(\frac{-L\ln 4 + M\ln x + 3}{2\sqrt{M}}\right) \\ &- \frac{2\text{erfc}\left(\frac{M\ln x - L\ln 4}{2\sqrt{M}}\right)}{3x^{3/2}}. \end{aligned} \quad \textbf{(20)}$$

In the case of $x \to \infty$, one has $\text{erf}(x) \to 1$ where $\text{erfc}(x) = 1 - \text{erf}(x)$. Therefore, $z(x)$ can be approximated as

$$z(x) \approx -\frac{2}{3}e^{-(3(L\ln 16 - 3))/4M} - \frac{2\text{erfc}\left(\frac{M\ln x - L\ln 4}{2\sqrt{M}}\right)}{3x^{3/2}}. \quad (21)$$

Then, by combining (19) and (21),

$$\begin{aligned}\bar{\varepsilon}_U \approx& \frac{D_{max}^3}{(D_{max}^3 - D_{min}^3)}\left(\text{erfc}\left(\frac{M\ln\left(\frac{W}{D_{max}^2}\right) - L\ln 4}{2\sqrt{M}}\right)\right. \\ &\left. - \text{erfc}\left(\frac{M\ln\left(\frac{W}{D_{min}^2}\right) - L\ln 4}{2\sqrt{M}}\right)\right). \end{aligned} \quad \textbf{(22)}$$

Table 1. System Parameters

Parameter	Value
Photodiode Responsivity (R_p)	0.4 mA/mW
Fixed Capacitance of PD (C_{pd})	112 pF/cm^2
Electron Charge (q)	1.6 $\times 10^{-19}C$
Channel Noise Factor(Γ)	1.5
Equivalent Bandwidth (B)	1 MHz
Open-Loop Voltage Gain (G_{ol})	10
Absolute Temperature (T_k)	300 K
Receiver Effective Area (A_r)	1 cm^2
Background Radiation (I_B)	0.04 A
Transconductance (g_m)	30 ms
Boltzmann's Constant (κ)	1.38 $\times 10^{-23}$J/K
Optical Depth (τ_{od})	0.7 [10]
Maximum distance among UAVs (D_{max})	20 m [46]
Minumum distance among UAVs (D_{min})	0.1 m
Default distance among UAVs (d)	10 m
Angle of incidence (ψ)	45^o
Angle of irradiance (φ)	45^o
LED semi-angle ($\varphi_{1/2}$)	45^o
Default packet size (L)	100 bits
Default blocklength (M)	200

D. Performance Metrics

This section explains the performance metric for LiFi-based UAV swarm networks in the case of ultra-reliability and low-latency communications. Consider $i = \{C, L, U\}$ as the different boundaries for the ABEP such as Chebyshev, lower and upper bounds, respectively.

Reliability, χ, refers to the probability of achieving successful packet delivery without experiencing any loss during transmission across the network. In essence, reliability and the packet loss rate (PLS) are completers of each other. That is $\chi + PLS = 1$, and reliability is given by [40]

$$\chi_i = (1 - \bar{\varepsilon}_i)100\%. \quad (23)$$

Throughput is the number of correctly determined information bits at the receiver per transmission, presented by [25]

$$T_i = R_s(1 - \bar{\varepsilon}_i). \quad (24)$$

Latency is the delay in transmission, given by [40]

$$l_i = MT_{max}/(1 - \bar{\varepsilon}_i). \quad (25)$$

4. NUMERICAL RESULTS

This section presents the performance of LiFi-enabled UAV swarm networks in terms of the analysis in Section 3. Chebyshev approximation, the lower and upper bounds are compared to show the limits of the proposed system by leveraging the SPC. Furthermore, the performance of the proposed LiFi-based UAV swarm networks is compared with benchmark RF-based UAV systems to demonstrate its efficacy [7, 25]. To validate findings,

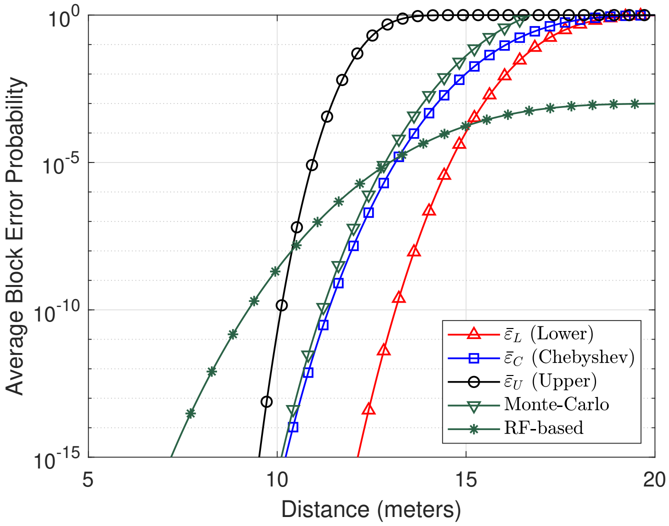

Fig. 3. The average block error probability (ABEP) values for different distances among UAVs.

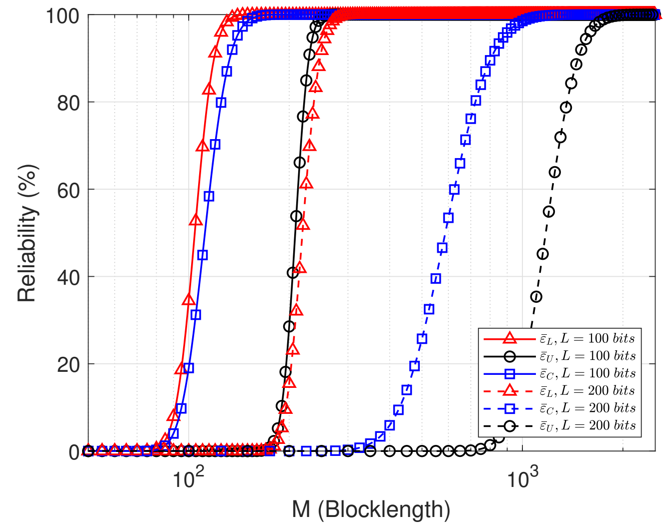

Fig. 5. The reliability of the packet lengths (100 bits and 200 bits) in terms of different blocklength regimes.

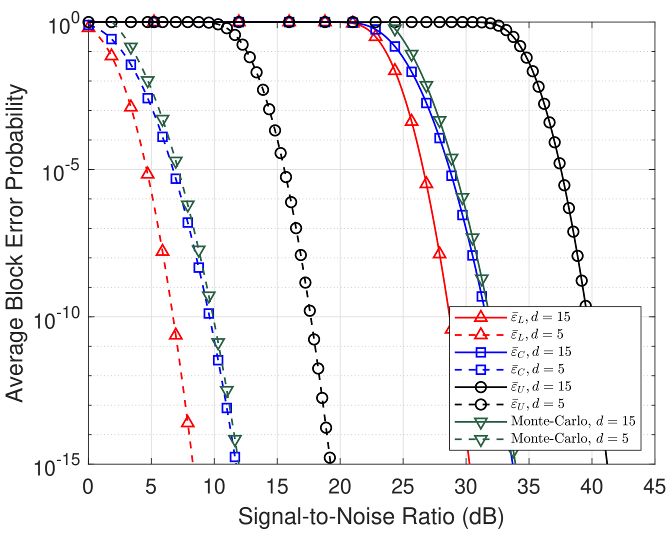

Fig. 4. The ABEP values of different boundaries for d={5, 15} meters.

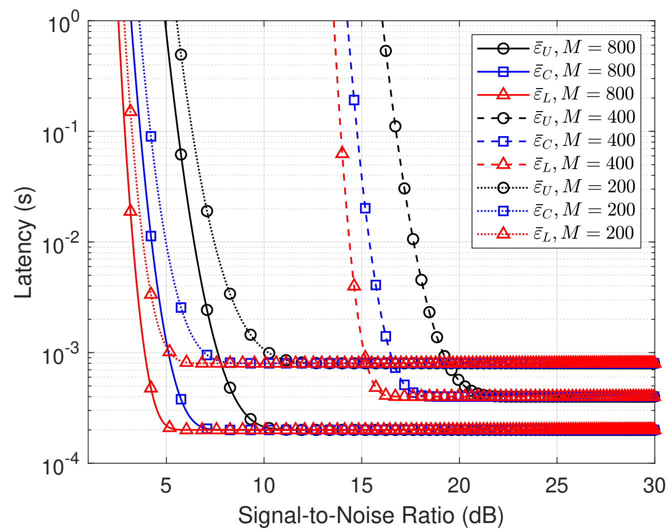

Fig. 6. The latency performance for the different values of the SNRs and blocklengths.

we conducted extensive Monte-Carlo simulations, deploying a vast number of UAVs randomly and uniformly in the designated region over 10^4 iterations. The closed-form analytical expressions are compared with the Monte-Carlo simulation results in MATLAB. Monte-Carlo simulation is a technique used to study how a model responds to randomly generated inputs. The ABEP, reliability, latency, and throughput results are discussed in the effect of the SNR, blocklength, and semi-angles of the LEDs. Unless otherwise stated, the system parameters are set as in Table 1. The curves labeled in figures as Chebyshev approximation ($\bar{\varepsilon}_C$), lower bound ($\bar{\varepsilon}_L$) and upper bound ($\bar{\varepsilon}_U$) are obtained by using (14), (18) and (22), respectively.

In Fig. 3, the evaluation of ABEP performance is presented for different approaches, considering variations in the distances among UAVs. The figure illustrates a notable observation that the error probability increases as the distance between UAVs increases, primarily due to higher path loss at longer distances. Furthermore, the comparison between Monte-Carlo simulation results and the analytical-based Chebyshev approximation reveals a close match. However, some slight gaps between these approaches exist, attributed to the inherent nature of the simulation technique and the approximation errors in the analytical expressions. This figure also provides a performance comparison between LiFi-based and RF-based UAV systems [7, 25]. This RF-based UAV channel has the free space channel model, which is for the scenario where the LoS dominates the environment. This channel model is valid when the UAV is deployed in an obstacle-free area, such as a big square, playground, large lawn, etc. It is also assumed that the transmission power between RF-based UAVs is fixed and the noise power at the UAV is denoted as σ^2. In short distances, LiFi systems exhibit better error probability performance, particularly under stringent la-

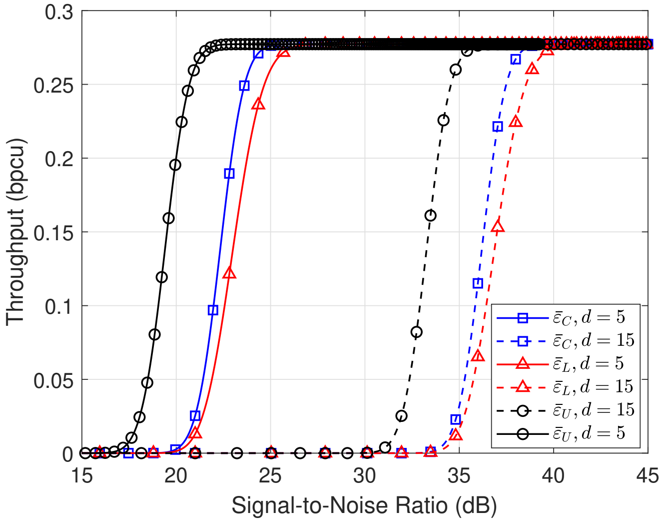

Fig. 7. The throughput of the SNR values for the different distances among UAVs.

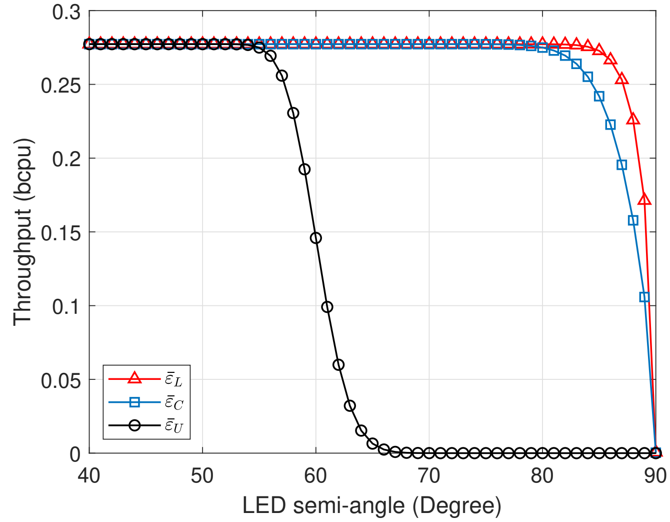

Fig. 8. The throughput for different values of semi-angles in different boundaries.

tency and reliability requirements. However, as the distance between UAVs increases, the LiFi-based approximations begin to exhibit inferior performance compared to RF-based systems. This observation can be attributed to the considerable path loss experienced by the LiFi communication channel over extended distances.

In Fig. 4, we investigate the effect of the SNR values and two different distances among UAVs together on the ABEP performance in terms of different boundaries. The choice of two different UAV distances, 5 meters and 15 meters, in the system model was primarily made to showcase two specific scenarios representing different levels of drone proximity. For example, drones are now commonly utilized in search and rescue missions, with their interplane distance tailored to the specific requirements of the operation. In rugged and densely vegetated search areas, a shorter interplane distance of 5 meters allows the drones to navigate challenging terrain carefully, capturing detailed images and sensor data. Conversely, in border or perimeter security tasks, where extensive coverage is paramount, drones are spaced at 15 meters to efficiently patrol large areas. These values were selected based on prior research [46] and practical considerations to illustrate the results under distinct distance configurations. It is observed that the ABEP with finite blocklength regime decreases with the increase of SNR as expected. Also, one can see from the figure that the boundaries in $d = 5$ m have better performance than in $d = 15$ m for the same boundaries at the same SNR value which shows that the ABEP decreases with the decrease of distance among UAVs for all boundaries. Our derived Chebyshev curve closely approximates the Monte-Carlo simulation results, demonstrating good matches between the analytical approach and the empirical simulations. Hence, these results can be used to estimate the trend of the ABEP. Besides, it is noted that the ABEP can be as low as 10^{-7} even in low SNR values, which satisfies the extreme reliability requirement.

In Fig. 5, we compare the reliability of the packet lengths (100 bits and 200 bits) in terms of different blocklength regimes. The chosen packet length values, $L = \{100,\ 200\}$ bits, are aligned with prior research [7, 25] and are employed to explore the effects of different packet lengths on the system performance. A packet length of 100 bits represents a relatively small packet size. Conversely, a packet length of 200 bits signifies a longer transmission duration, leading to larger data packet sizes." The reliability is calculated as the function of the total blocklength at $\gamma_r = 20$ dB. The reliability of short messages is higher than the long ones. The 100 bits packets can satisfy the reliability requirement with more than $M = 200$ while the 200 bits packets need more than $M = 1000$ to satisfy the ultra-reliability requirement which is more than 99.99% for 5G and beyond systems.

In Fig. 6, the latency performance is given for the different values of the SNRs and blocklenghts ($M = 200, 400, 800$ bits). The latency performance of the longer blocklengths is lower than short ones for the same packet length ($L = 100$ bits) because the longer blocklengths (size of coded packet) provide a larger capacity for packet transmission. Also, the longer blocklength regimes need higher SNR values for ensuring the latency requirement. The system also reaches the sub-millisecond latency which is quite enough for low-latency communication in UAV networks.

In Fig. 7, we plot the throughput versus SNR for the different distances among UAVs. Actually, it follows similar trends as Fig. 4 because throughput is directly connected with the ABEP values as seen from (24). Throughput increases with the increase of the SNR and reaches the roof with the further increase of SNR.

Fig. 8 depicts the throughput of the system with various semi-angles of the LED. As shown in (3), the channel gain depends on the Lambertian radiation pattern which is subject to the semi-angle of the LED. Since the throughput of the system depends on the channel gain, the semi-angle of the LED relates to the throughput. At $\gamma_r = 25$ dB and $d = 5$ m, the throughput of the LiFi-enabled UAV system can achieve maximum for all boundaries until 57^o semi-angle. The greater values of the semi-angle of the LED deteriorate the system performance. Generally, the Chebyshev approximation is tighter to the lower bound due to the influence of the Legendre polynomials in (14). As the power of the approximation increases, its accuracy can also improve, albeit with a corresponding increase in computational requirements.

It is also to be highlighted that this paper is a preliminary work for infrared/visible bands-based LiFi technology for enabling strict reliability and latency requirements in relaying systems among UAVs. Thus, a suitable algorithmic approach for LiFi-based UAV swarm networks or a more realistic system model will be the subject of further studies. The obtained results show that the LiFi-based method has the potential for UAV swarm in future networks and is worth investigating deeper.

5. CONCLUSION

In this study, it is proposed to use LiFi, a light-spectrum-based wireless system, as a potential non-3GPP technology that brings advantages in communication relaying among UAVs in terms of ultra-reliability and low-latency. After the explanation of the system model in terms of the network model, channel characteristics, and short packet transmission in LiFi, we have derived three different expressions of the ABEP which are the Chebyshev approximation, lower bound, and upper bound. Moreover, the reliability, latency, and throughput expressions are obtained thanks to the ABEP derivations. Thus, it is shown that the LiFi-enabled system provides ultra-reliability and low-latency for UAV swarm networks. Future work will focus on different scenarios and system models.

Funding. H2020 Marie Skłodowska-Curie Actions (814215, ENLIGHT'EM:Low-Energy Visible Light IoT Systems).

Disclosures. The authors declare no conflicts of interest.

Data availability. No data were generated or analyzed in the presented research.

REFERENCES

1. G. Chen, T. Wu, F. Yang, *et al.*, IEEE Wirel. Commun. pp. 1–8 (2022).
2. I. O. Committee, "Spectacular intel drone light show helps bring tokyo 2020 to life - olympic news," (2022).
3. C. Yao, H. Tian, C. Wang, *et al.*, IEEE Wirel. Commun. **28**, 28 (2021).
4. Z. Yuan, J. Jin, L. Sun, *et al.*, IEEE Commun. Mag. **56**, 90 (2018).
5. J. Sachs, G. Wikstrom, T. Dudda, *et al.*, IEEE Netw. **32**, 24 (2018).
6. A. Masaracchia, Y. Li, K. K. Nguyen, *et al.*, IEEE Access **9**, 137338 (2021).
7. H. Ren, C. Pan, K. Wang, *et al.*, IEEE Wirel. Commun. Lett. **8**, 1587 (2019).
8. C. M. W. Basnayaka, D. N. K. Jayakody, and Z. Chang, IEEE Internet Things J. **9**, 10212 (2022).
9. A. Ranjha, G. Kaddoum, and K. Dev, IEEE Trans. on Ind. Informatics **18**, 4954 (2022).
10. Z. Ghassemlooy, W. Popoola, and S. Rajbhandari, *Optical wireless communications: system and channel modelling with Matlab®* (CRC press, 2019).
11. N. Chi, Y. Zhou, Y. Wei, and F. Hu, IEEE Veh. Technol. Mag. **15**, 93 (2020).
12. P. H. Pathak, X. Feng, P. Hu, and P. Mohapatra, IEEE Commun. Surv. Tutorials **17**, 2047 (2015).
13. K. Chen, Y. Wang, Z. Fei, and X. Wang, "Power limited ultra-reliable and low-latency communication in uav-enabled iot networks," in *2020 IEEE Wireless Communications and Networking Conference (WCNC),* (2020), pp. 1–6.
14. R. Islambouli and S. Sharafeddine, IEEE Access **7**, 172860 (2019).
15. N. Abbas, A. Mrad, A. Ghazleh, and S. Sharafeddine, IEEE Netw. Lett. **3**, 110 (2021).
16. C. She, C. Liu, T. Q. S. Quek, *et al.*, "Uav-assisted uplink transmission for ultra-reliable and low-latency communications," in *2018 IEEE International Conference on Communications Workshops (ICC Workshops),* (2018), pp. 1–6.
17. L. Yuan, N. Yang, F. Fang, and Z. Ding, IEEE Trans. on Veh. Technol. **71**, 4471 (2022).
18. K. Chen, Y. Wang, J. Zhao, *et al.*, IEEE Internet Things J. **8**, 10103 (2021).
19. H. Ren, C. Pan, K. Wang, *et al.*, IEEE Trans. on Veh. Technol. **69**, 8003 (2020).
20. Y. Cai, X. Jiang, M. Liu, *et al.*, IEEE Trans. on Veh. Technol. **71**, 3344 (2022).
21. A. Ranjha and G. Kaddoum, IEEE Wirel. Commun. Lett. **9**, 306 (2020).
22. P. Yang, X. Xi, T. Q. S. Quek, *et al.*, IEEE Wirel. Commun. Lett. **10**, 1018 (2021).
23. C. Pan, H. Ren, Y. Deng, *et al.*, IEEE Commun. Lett. **23**, 498 (2019).
24. A. Han, T. Lv, and X. Zhang, "Uav beamwidth design for ultra-reliable and low-latency communications with noma," in *2019 IEEE International Conference on Communications Workshops (ICC Workshops),* (2019), pp. 1–6.
25. K. Wang, C. Pan, H. Ren, *et al.*, IEEE Trans. on Commun. **69**, 73 (2021).
26. J. Jayaraman, V. R. Balu, S. Bregni, *et al.*, "Rooftop relay nodes to enhance urllc in uav-assisted cellular networks," in *ICC 2022 - IEEE International Conference on Communications,* (2022), pp. 733–738.
27. A. Qazavi, F. S. Tabataba, and M. N. Soorki, "Joint user association and uav location optimization for two-tired visible light communication networks," in *2022 30th International Conference on Electrical Engineering (ICEE),* (2022), pp. 755–761.
28. Y. Yang, M. Chen, C. Guo, *et al.*, IEEE Commun. Lett. **23**, 1272 (2019).
29. Z. Zhu, Y. Yang, C. Guo, *et al.*, "Power efficient deployment of vlc-enabled uavs," in *2020 IEEE 31st Annual International Symposium on Personal, Indoor and Mobile Radio Communications,* (2020), pp. 1–6.
30. Y. Wang, M. Chen, Z. Yang, *et al.*, IEEE Trans. on Wirel. Commun. **19**, 7049 (2020).
31. R. Feng, Z. Li, Q. Wang, and J. Huang, IEEE Wirel. Commun. Lett. **11**, 1123 (2022).
32. D. N. Anwar, M. Peer, K. Lata, *et al.*, IEEE Trans. on Green Commun. Netw. pp. 1–1 (2022).
33. J. Ye, C. Zhang, H. Lei, *et al.*, IEEE Wirel. Commun. Lett. **8**, 564 (2019).
34. M. D. Soltani, A. A. Purwita, Z. Zeng, *et al.*, IEEE Trans. on Commun. **67**, 2157 (2019).
35. M. S. Islim, S. Videv, M. Safari, *et al.*, J. Light. Technol. **36**, 2376 (2018).
36. F. M. Davidson and X. Sun, IEEE Trans. on Commun. **36**, 1185 (1988).
37. A. B. Ozyurt and W. O. Popoola, J. Opt. Commun. Netw. **13**, 204 (2021).
38. A. B. Ozyurt and W. O. Popoola, IEEE Syst. J. pp. 1–8 (2022).
39. A. B. Ozyurt and W. O. Popoola, IEEE Access **10**, 70760 (2022).
40. G. N. Tran and S. Kim, IEEE Access **10**, 6505 (2022).
41. G. Durisi, T. Koch, and P. Popovski, Proc. IEEE **104**, 1711 (2016).
42. Y. Polyanskiy, H. V. Poor, and S. Verdu, IEEE Trans. on Inf. Theory **56**, 2307 (2010).
43. M. Abramowitz, Graphs, Math. Tables (1965).
44. S. Zlobec, Math. Commun. **9**, 119 (2004).
45. W. R. Inc., "Mathematica, Version 13.1," Champaign, IL, 2022.
46. Y. Cang, M. Chen, J. Zhao, *et al.*, IEEE Trans. on Wirel. Commun. pp. 1–1 (2022).